

# A Lightweight Rotary Spring Design, Part I: Linearly Stiffening Springs

Zachary Bons<sup>†</sup>, *Student Member, IEEE*, Gray C. Thomas<sup>†</sup>, *Member, IEEE*, Luke Mooney, Elliott Rouse, *Senior Member, IEEE*

**Abstract**—Springs are important machine components in many industries, with compactness, mass, and flexible specification of the spring rate all desirable attributes. This paper presents a novel rotary spring design concept that is both light and compact. The approach uses simplifying assumptions to design springs without requiring a full finite element model. Three linear test springs validate the achievement of target spring rates and deflections in an automated dynamometry testbed.

## I. INTRODUCTION

**S**PRINGS are essential building blocks for many mechanical engineering applications. Apart from their varied use in latches, clutches, scales, suspensions, oscillators, and more, springs are often used to store elastic energy and measure force or torque; actuators that implement a spring between the output of the transmission and the load are known as Series Elastic Actuators (SEAs) [1], which have gained prominence in human-centered robotic applications [2]–[4]. Though not without drawbacks—namely force bandwidth reduction as well as increased mass and complexity—this design paradigm has notable benefits, including compliant interaction with the environment, torque feedback, energy storage, and improved shock tolerance. In recent years, the SEA application has become a driving force in torsion spring designs. For mobile robot systems, these designs have prioritized specific energy (energy storage per mass) and energy density (energy storage per volume).

Simple torsion spring designs, including thin-walled tubes and cantilever beams, have posed challenges in packaging and volume within SEA designs. Torsion tube springs with thin walls [5], [6] and long beam flexures with cam-rollers [7] or hinges [8] can be effective while maintaining a low stiffness, and their low weight results in high specific energy. However, to achieve appropriate stiffness values, the aspect ratio—length over diameter—must be considerable [9]. Thus, tubular geometries are often impractical for rotary joints in robots. This challenge has resulted in an era of spring designs that prioritize convenient packaging in addition to specific energy and energy density.

To achieve convenient packaging, recent designs have emphasized disk-like architectures that balance specific energy,

compactness, and required mechanics. These springs incorporate torsional elasticity between a central anchor point rotated with respect to an outer rim (Fig. 1). Some early researchers achieved this design by arranging prismatic springs tangentially around a circular frame [10], [11]. However, this approach results in a nonlinear stiffness behavior [11] and has the added complexity of removable parts. The latter concern may be responsible for the transition to monolithic springs in subsequent designs. One of the most common and successful planar monolith spring designs connects the central anchor to the rim with one or more spiral arms [12]–[17]. This configuration is efficient and works well with a wide range of stiffness coefficients (*e.g.* 30–800 Nm/rad); however, the

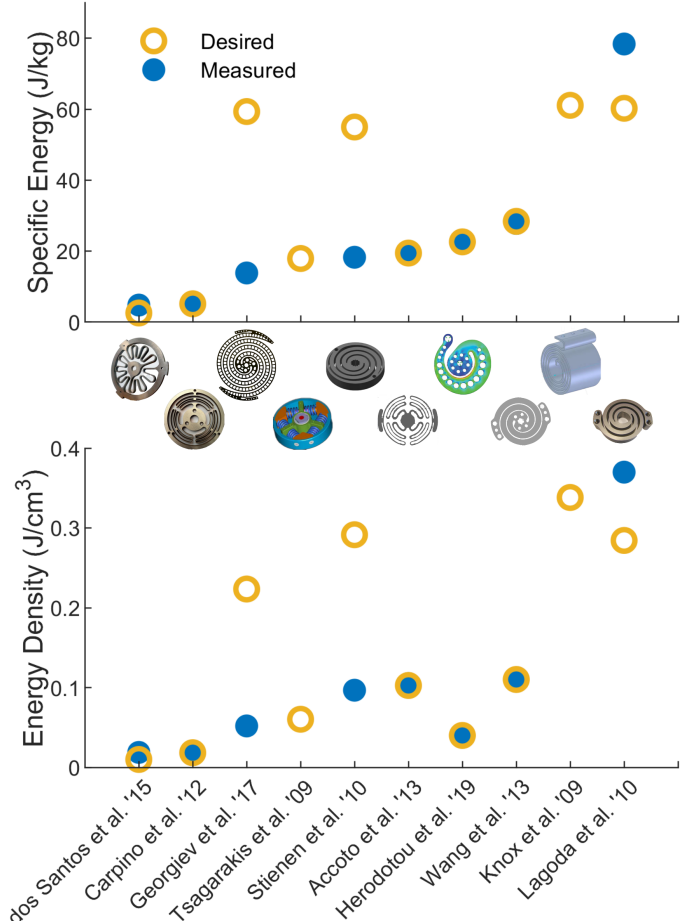


Fig. 1. Performance of torsional springs across the literature by energy storage per unit mass (specific energy) and per unit volume (energy density).

(Z. Bons' e-mail: zbons@umich.edu).

Manuscript not yet submitted Monthmonth X, 20XX; nor revised.

<sup>†</sup> — co-first authors

Color versions of one or more of the figures in this paper are available online at <https://ieeexplore.ieee.org>.

Digital Object Identifier XX.XXXX/SRO.2019.XXXXXXX

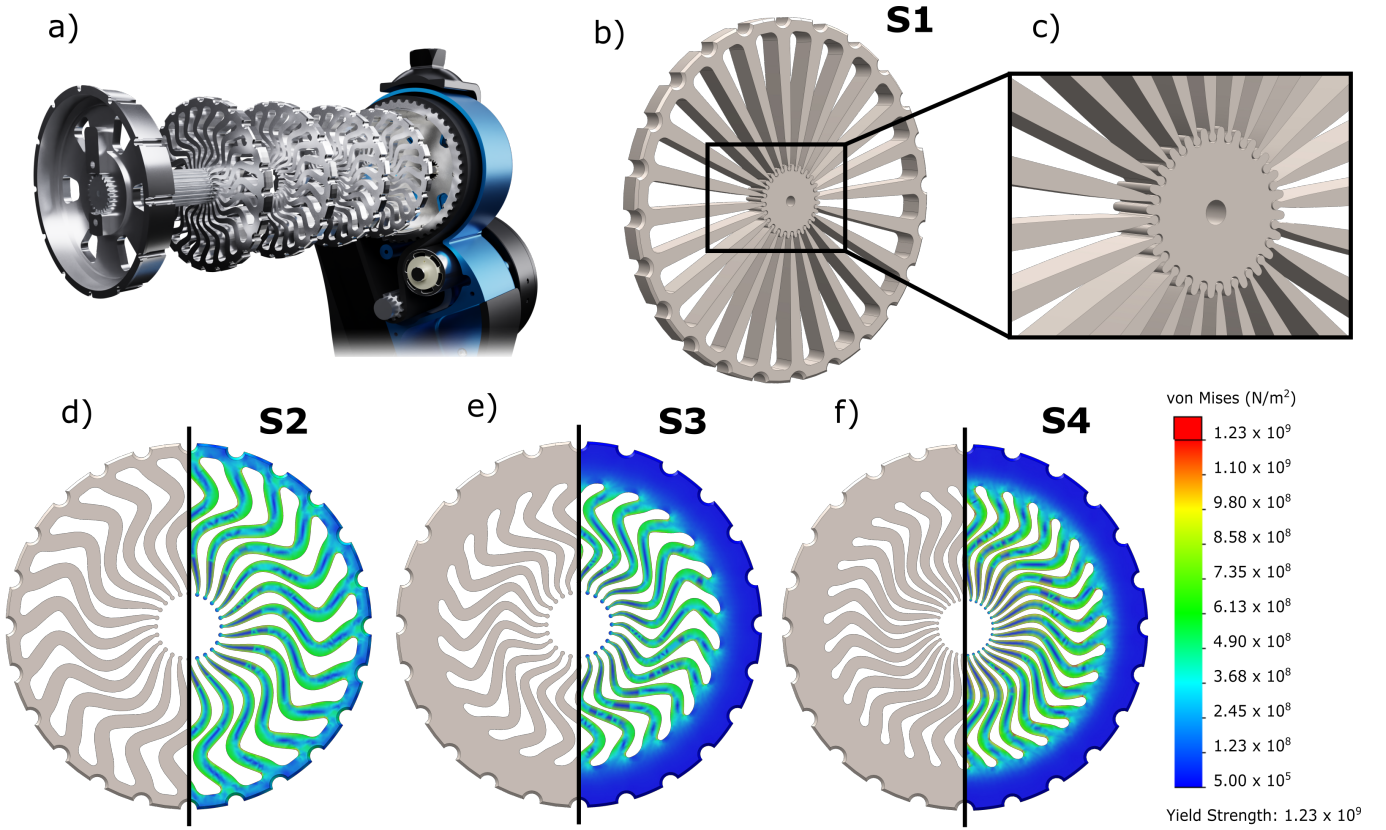


Fig. 2. Rotary spring design based on bending cantilever flexures. a) the spring neatly mates with transmission components—in this case, a belt pulley in the Open-Source Leg. b) the original design consists of straight flexures with a tapered profile. c) the flexures mate with a gear-like camshaft, which loads the spring when rotated. d) and e) later designs feature serpentine flexures in addition to the tapered profile. f) we also optimized the number of flexures for maximal energy storage in the spring.

nature of the spiral arms often causes differences in stiffness depending on the direction of deflection [17]. Other designers have emphasized torque-sensing resolution [18]–[24] in their development. These designs have produced compact springs that are limited in their overall deflection (*e.g.* less than five degrees), which has diminished their success in many SEA applications. While the overall spring performance has been well-predicted in some cases [15], [16], the directionality and limited range of motion are drawbacks of these approaches.

One method to improve the energy density of springs is to modify the loading condition of the elastic elements within the spring. That is, the above-mentioned rotary spring designs fully constrain both ends of the spring, which prevents the material from achieving ideal bending, leading to lower energy density and specific energy of the final spring. One way to shift towards more efficient loading conditions is to develop springs that can be assembled from multiple parts. For example, Herodotou *et al.* proposed a novel design in which one end of the arm is fixed and the other end is hinged [25]. This design is quite efficient (by mass) and the stiffness was accurately predicted by models and FEA. Drawbacks of these designs are that they add complexity, and have thus far only been developed for extremely high stiffness values (1950 Nm/rad); however, it is possible that lower stiffness behaviors could be achieved with a similar strategy.

Despite impressive spring performance across previous

work, each of these design paradigms is limited in some respect. A spring design that fully exploits an efficient loading condition should be capable of achieving low stiffness behaviors while also maintaining a compact form-factor and low mass. In addition, a design that employs a convenient mate with transmission components (*e.g.* fitting inside the timing belt pulley of a belt-drive transmission [26]) would be novel and desirable. Inspired by Ref. [27], we developed a two-element planar spring design, that addresses these gaps, is predictable and customizable, and has high energy-per-mass and energy-per-volume efficiency (Fig. 1).

In this paper we 1) introduce a compact and lightweight rotary spring design based on simple design indices, 2) present a design tool for generating spring profiles from the design indices, and 3) empirically validate three representative test spring designs. These contributions enable rapid adoption of an energy-efficient spring design and thus pave the way for lighter-weight and more compact technologies.

## II. SPRING DESIGN

In this section, we introduce the design of our spring topology (Fig. 2) and provide the governing equations that describe the mechanics and geometry of the individual flexures. Our intent is to motivate the rationale for our design decisions, as well as provide a guide for other researchers to modify for other applications. In addition, we have developed a spring

design tool and graphical user interface (see Section III), which is openly-available in [REF].

Our spring design (Fig. 3a) comprises a gear-like camshaft in contact with a ring of radial flexure teeth. The teeth protrude inward from a shared outer ring, which is fixed to the spring housing. When the camshaft rotates, a contact force is imposed on the tip of each tooth. The camshaft and tooth tip are both designed to result in an applied force that is nominally perpendicular to the length of each flexure. In operation, the gear-like camshaft rotates relative to the rim ring, causing each of the inward-pointing flexures to bend like a cantilever beam. The spring is fixed in place using dowel rods that oppose rotation between the spring and the inner bore of the housing.

#### A. Straight Tapered Flexures

To maximize the specific energy, each inward-pointing flexure is tapered. The tapering law [28] ensures that each cross section of the beam remains in ideal bending, and that the entirety of the two bending surfaces (Fig. 3b) reach the desired design stress at peak deflection. This tapering law governs  $\lambda$  (see Fig. 3b) as a function of  $x$  (the distance along each flexure), and is derived from basic beam-bending mechanics [29].

For a generic beam, we know  $\sigma = \frac{M\lambda}{I}$ , with  $\sigma$  as axial stress,  $M$  as applied moment ( $F(L - x)$  for our loading condition),  $\lambda$  as the distance from the neutral axis to the edge

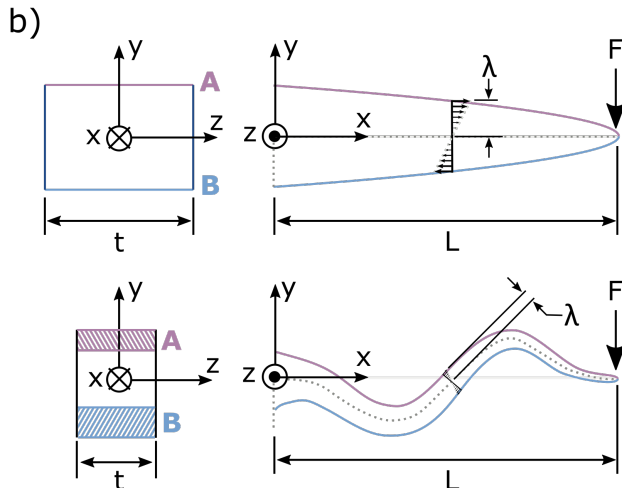
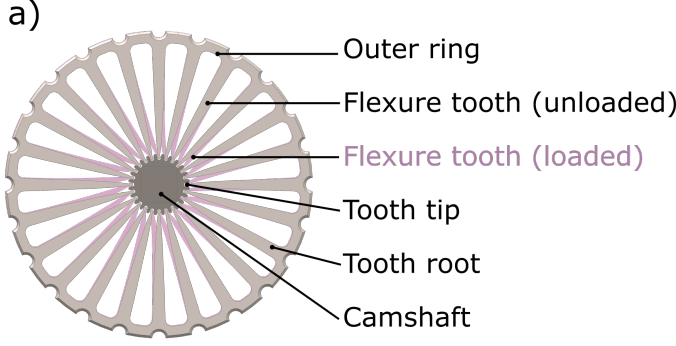


Fig. 3. a) Spring w/ labeled parts. b) Schematic of beam coordinate frames and loading condition. Surfaces A and B are the bending surfaces.

of the beam (see Fig. 3b), and  $I$  as the second moment of area. In the case of a planar spring, we have  $I = \frac{2t\lambda^3}{3}$ , with  $t$  as the thickness of the spring (see Fig. 3b). To achieve maximum stress along the length of the beam, we choose  $\lambda$  at each cross-section such that  $\sigma = \sigma_d$ :

$$\sigma_d = \frac{3F(L - x)\lambda}{2t\lambda^3}, \quad (1)$$

$$\lambda(x) = \sqrt{\frac{3F(L - x)}{2t\sigma_d}}. \quad (2)$$

This tapering law can be used to relate spring rate and bending strain energy, which allows us to calculate the energy storage potential of the flexures and overall spring. Three governing assumptions simplify the analysis: we assume that the applied force is perpendicular to the length of each flexure, the spring only deflects at small angles, and every cross-section of each flexure is in ideal bending.

With the aforementioned assumptions in place, we can easily calculate strain energy. For a generic beam in bending, strain energy ( $U$ ) is defined by  $U = \frac{M\theta}{2}$ , with  $M$  as previously defined and  $\theta$  as deflection angle. We also know that  $\theta = \kappa L$ , where (curvature)  $\kappa = \frac{M}{EI}$ . Thus, we see that  $U = \frac{M^2 L}{2EI}$ . For a varying beam profile with small deflections, we can rewrite strain energy as follows:

$$U = \int_0^L \frac{F^2(L - x)^2}{2EI} dx. \quad (3)$$

Substituting our definitions of  $I$  and  $\lambda$  yields

$$U = \int_0^L \frac{3F^2(L - x)^2}{4Et\sqrt{\frac{3F(L-x)}{2t\sigma_d}}} dx. \quad (4)$$

Rearranging and simplifying,

$$U = \frac{\sigma_d^2 t}{3E} \int_0^L \sqrt{\frac{3F(L - x)}{2t\sigma_d}} dx, \quad (5)$$

which can be rewritten in closed form as

$$U = \sqrt{\frac{2tFL^3\sigma_d^3}{27E^2}}. \quad (6)$$

Since force ( $F$ ) is a function of stiffness ( $k$ ), desired deflection ( $\theta_{des}$ ), the number of flexures ( $n$ ) and the flexure-camshaft contact radius ( $r$ ), this can be further simplified to

$$U = \sqrt{\frac{2tk\theta_{des}L^3\sigma_d^3}{27E^2rn}}. \quad (7)$$

By itself, the tapering law characterizes mass-efficient straight flexures. However, with this parameterization, specific stiffness ( $k$ ), geometry ( $r, L, n, t$ ) and material ( $E, \sigma_d$ ) constraints directly limit the possible deflection of the spring (Eq. 7). The density of the spring disks is also limited due to the necessary gaps between flexures to accommodate deflection and the gear-like cam shaft.

### B. Serpentine Tapered Flexures

To maximize energy density while maintaining high specific energy, it is possible to design *serpentine* flexures that follow the tapering law. This results in beams that are effectively longer than the *straight* flexures, yielding higher energy storage (deflection) for the same outer diameter. A serpentine design also makes better use of the gaps between flexures, resulting in higher overall volume-efficiency in comparison to the straight flexure designs.

To parameterize the design of serpentine flexures, we first rewrite the expression for strain energy (Eq. 5) by substituting our definition of  $\lambda$  (Eq. 2),

$$U = \frac{1}{6} \frac{\sigma_d^2}{E} t (2 \int_0^L \lambda dx), \quad (8)$$

which can be further generalized to

$$U = \frac{1}{6} \frac{\sigma_d^2}{E} t A. \quad (9)$$

Energy storage is therefore a function of the planar area of the flexures, so by appropriately increasing the area of the flexure, we can increase energy storage. Assuming that we design a spring with specified stiffness and diameter and desired deflection properties, we can calculate desired energy storage for a single beam,  $\mathcal{E} = \frac{1}{2n} k \theta_{des}^2$ . By equating  $\mathcal{E}$  and the strain energy ( $U$ ), we easily determine the required planar area ( $A_{serp}$ ) of a flexure that achieves our desired peak deflection and torque,

$$A_{serp} = \frac{3k\theta_{des}^2 E}{n\sigma_d^2 t} \quad (10)$$

Therefore, knowing the required planar area ( $A_{serp}$ ) and the governing tapered profile, one can define a serpentine flexure that satisfies the constraints. To aid in classification of a spring with such flexures, we introduce two design indices that indicate feasibility of a spring.

- **Serpentine factor ( $f_s$ ):** The serpentine factor is calculated as  $f_s = \frac{A_{serp}}{A_{nom}}$ , where  $A_{nom}$  is the planar area of the straight flexures—and describes the sinuosity of a given flexure. If  $f_s = 1$ , then the desired spring will have straight flexures. If  $f_s < 1$ , the flexure is undefined, and the diameter of the spring can be decreased while still maintaining the required deflection. Lastly, if  $f_s > 1$  flexures should have a serpentine shape in order to achieve desired performance.
- **Density factor ( $f_d$ ):** A density factor is calculated as  $f_d = \frac{A_{serp} n}{A_{annulus}}$ , where  $n$  is the number of flexures in the spring and  $A_{annulus}$  is the annular (donut-shaped) area in which the flexure teeth lie. This indicator describes the compactness of the flexures within the the spring: a value of 1 would indicate that the spring is a solid disk (all flexures are touching) whereas a value of 0 would represent a spring with no flexure teeth. In the testing performed, we have had difficulty designing springs that don't self-intersect with  $f_d > 0.55$ .

### C. Additional Factors

Several other design parameters have large effects on energy-storage potential, namely the number of flexures and the flexure-camshaft contact radius. First, increasing the number of flexures within the spring reduces the empty space between flexures—similar to the serpentine concept—and thus increases energy density. Second, decreasing the contact radius makes space for longer flexures, and therefore also increases the energy density of the spring.

The direct relationship between these parameters and spring deflection can be seen by again equating desired energy storage,  $\mathcal{E}$ , and the strain energy,  $U$ . Using strain energy as defined in Eq. 7 and solving for spring deflection yields

$$\theta_{des} = \sqrt[3]{\frac{8tnL^3\sigma_d^3}{27E^2kr}}. \quad (11)$$

Thus, even when all geometry and material parameters are constrained, increasing the number of flexures ( $n$ ) further increases deflection and therefore energy storage. Similarly, decreasing contact radius ( $r$ ) directly improves deflection, but it also increases  $L$  ( $L = R - r$ ) which in turn increases spring deflection. Thus, proper selection of these parameters can greatly enhance spring performance. Practical limitations typically govern the possible number of flexures and a feasible contact radius (e.g. nearness constraints of flexure tips) which are described in Section III.

To summarize, by designing springs with the *optimal number* of *serpentine* flexures with a *tapered* profile, we can achieve high energy storage per unit mass and volume.

### III. SPRING DESIGN TOOL

Using software, we can automatically design a spring profile that meets desired specifications using constrained nonlinear optimization to achieve the target planar flexure area. We developed this tool to enable quick and simple adoption of this new spring design in order to lower the barrier to entry for devices with custom elastic elements (scripts and instructions available @CODE OCEAN). The published library includes more specific documentation for its use in the MATLAB language, and generates output files that can be loaded into complete computer aided design packages like SolidWorks as a 2D sketch component from which the solid body of the spring can be extruded.

The primary objective of our automatic profile generation tool is to design a spring flexure that has the desired serpentine factor ( $f_{s,des}$ ) and thickness profile, thereby meeting the performance requirements of the spring. The spring designs are parameterized in such a way that the planar area (and thus the serpentine factor, stiffness, and total stored energy) can be adjusted by the constrained nonlinear optimization without increasing the packaging volume of the spring. As a secondary optimization objective, the spring design tool automatically generates a spring that is well suited to satisfy the assumptions made during the derivation of the design. Since planar area can be added to the spring in many different ways, the optimization is under-defined without these secondary objectives. Thus our tool can select flexure configurations with straight tips, straight

roots, laterally balanced geometry, smooth curves, and low probability of self-collision in addition to the planar area requirement.

Our spring geometry is parameterized by the center curve and the thickness profile. The center curve is defined using a cubic spline interpolation with end conditions. Splines were chosen for their robust manipulability. The end conditions pre-define the desired zero-slope conditions (see XY-plane in Fig. 3b) at both the tip and the root of the flexure, while the interior control points allow precise manipulation of the shape between the two ends. To limit the complexity of the optimization problem, the number of control points (not including the end points) is a user-defined input. We recommend starting with two or three, increasing as needed for springs with a high serpentine factor. The user also specifies the overall packaging format of the spring, including the outer radius of the flexure disk and the nominal radius of the gear-like camshaft. Points  $(x_{edge}, y_{edge})$  along the boundary of the flexure area are technically defined by moving a distance of  $\lambda$  (Eq. 2) in the direction perpendicular to the slope ( $m$ ) of the spline at each point  $(x_c, y_c)$  along the center curve:

$$\begin{bmatrix} x_{edge} \\ y_{edge} \end{bmatrix} = \begin{bmatrix} x_c \\ y_c \end{bmatrix} \pm \begin{bmatrix} 1 \\ -m \end{bmatrix} sgn(m) \frac{\lambda(x_c)}{\sqrt{m^2 + 1}}. \quad (12)$$

Area is computed numerically using a high-resolution approximation of the flexure curve.

Due to the presence of many local minima in our objective function (which complicates convergence to a global optimum), we include run-time as a user-defined input, and restart the optimizer repeatedly from randomized initial conditions until time runs out. The optimization is implemented using MATLAB's fmincon, and the large number of computations cause it to take several seconds to solve one set of initial conditions. We tested the implementation on a 4-core processor @ 1.50 GHz and we have found that setting the run time to 60 seconds allows the tool to find several viable spring designs. The final spring design is then automatically selected from the solutions of all trials.

Several constraints ensure a feasible solution of the nonlinear optimization. These constraints use a 2D coordinate system with x pointing outward from the center of the spring disk along the nominal center of the flexure.

- The x-coordinates of the  $n$  interior control points are constrained to be in descending order.
- The corresponding y-coordinates are constrained to the range  $[-\frac{L}{2}, 0]$  or  $[0, \frac{L}{2}]$  for odd or even points, respectively. This forces the spline to be roughly centered about the x-axis.
- The flexure face is constrained to have exactly the desired planar area. As shown in the characterization of the spring design, this is necessary to achieve desired spring performance. It is implemented by limiting the difference between the desired and actual serpentine factors ( $f_{s,des}$ ,  $f_s$ ):

$$|f_{s,des} - f_s| < 0.001. \quad (13)$$

- The spring is also constrained to be laterally balanced across the x-axis, which ensures that the spring will have

similar performance in both loading directions. This is implemented as follows, where  $n_c$  is the number of points along the centerline spline and  $y_{c,i}$  is the  $i$ th y-coordinate along that spline:

$$\left| \sum_{i=1}^{n_c} y_{c,i} \right| < 0.001. \quad (14)$$

The cost function is defined to penalize a combination of the sharpness of curvature and nearness to self-collision between flexures. Eliminating sharp curves is necessary to avoid the nonlinearities associated with stress concentrations. This is achieved by penalizing high curvature along the centerline spline. Curvature is calculated numerically and the sum of the squares of the curvature is included in the cost,

$$c_{\text{sharpness}} = \left| \sum_{i=1}^{n_p} K_i^2 \right|. \quad (15)$$

Collision of neighboring flexures leads to premature failure of the spring, so the best spring will have a large minimum distance ( $d_{min}$ ) between neighboring flexures. The minimum distance is calculated by checking the distance between every point along neighboring curves. The minimum is then stored, and its inverse is added to the cost, making small distances expensive:

$$c_{\text{nearness}} = \frac{1}{d_{min}}. \quad (16)$$

Total cost is then calculated as a weighted sum of  $c_{\text{sharpness}}$  and  $c_{\text{nearness}}$ .

We utilized this tool to design the springs used in the experimental validation of this spring design. An empirical evaluation of said springs is found in the following section of this paper.

#### IV. HARDWARE VALIDATION OF SPRING DESIGN FRAMEWORK

In this section, we empirically validate our design framework by comparing four springs with differing geometries and identical desired stiffness coefficients (Fig. 2). The four springs intentionally employ different serpentine factors and root radii (e.g. differing effective spring diameters) to highlight the impact of the flexure geometry on spring stiffness and energy storage capacity. Specifically, the springs tested in this study were as follows (Table I):

- **Spring One (S1)** was manufactured with straight flexures and a 31 mm root radius and serves as a baseline comparison for the other designs.
- **Spring Two (S2)** was designed to show that using serpentine flexures can increase allowable deflection compared to S1. It was manufactured with a moderate serpentine factor of 1.24, and a 31 mm root radius—equivalent to that of S1.
- **Spring Three (S3)** was designed to show that serpentine flexures enable similar performance to S1 within a smaller enclosed volume. It was manufactured with an aggressive serpentine factor of 1.32, but with a 26 mm root radius—substantially smaller than that of S1 and S2.

TABLE I

DESIGN PARAMETERS EXPECTED PROPERTIES OF THE FOUR SPRINGS. THE MASS OF ALL FOUR SPRINGS WAS CALCULATED ASSUMING A 2.5MM THICK RIM CONNECTING ALL FLEXURES ON THE OUTER EDGE.

Spring Design	Spring Rate (Nm/rad)	Desired Deflection (deg)	Mass (g)	Root Radius (mm)	Contact Radius (mm)	Number of Flexures	Serpentine Factor	Density Factor	Cycles to Failure
S1	150	12.6	57.3	31.0	6.0	24	1.00	0.40	100,000
S2	150	14.5	71.0	31.0	6.0	24	1.24	0.53	100,000
S3	150	12.1	51.8	26.0	6.0	24	1.32	0.53	100,000
S4	150	13.4	60.1	26.0	5.1	31	1.17	0.64	100,000

- **Spring Four (S4)** was designed to demonstrate the combined effect of using serpentine flexures after optimizing the number of flexures and the flexure-camshaft contact radius for maximum deflection. It has a light serpentine factor of 1.17, 31 flexures, a 5.1 mm contact radius and the same 26 mm root radius as S3.

All four springs were manufactured from SS420, and were designed with a target spring rate of 150 Nm/rad, spring thickness of 4.5 mm, and identical outer radius (33.5 mm) to interface with the spring housing.

### A. Methods

The purpose of this experimental protocol was to empirically validate our spring design approach. We characterized the stiffness of four springs designed to have identical stiffness values. Our experimental apparatus (Fig. 4) deflected the spring by actively using two opposing actuators, while simultaneously measuring the deflection and torque at the spring interface. The springs were held in a housing with complementary semi-circular cutouts on the inner bore. The applied moments were opposed by inserting dowel rods in the circular cutouts at eight evenly-spaced locations around the spring. Torque was measured with a contactless sensor (#, Futek, Irvine CA) in series with the spring assembly. The torque sensor output an analog voltage that was sampled by an XX-bit analog-to-digital converter at XX Hz. Rotary motion was provided by two identical brushless DC actuators (ActPack, Dephy Inc, Maynard MA), each coupled to a transmission (50:1 PL2090-050, Boston Gear, Boston MA), as used in [30]. The actuators were controlled in current or position control modes by a microprocessor (RPi 3 Model B+, Raspberry Pi Foundation, Cambridge UK). Both actuators include an encoder, however deflection within the transmission and testbed setup required obtaining spring deflection separately.

Spring deflection was directly measured using a custom optical encoder and image processing algorithm. Two arrays of optical fiducials were used for the measurement: one set was rigidly mounted to the shaft that engaged the spring, while the other set was fixed to the spring housing. Tracking these two fiducial arrays, enabled more accurate measurement of the total spring deflection.

A dedicated high-definition camera provided input to our image processing algorithm. An HD digital camera (RPi Camera Module 2, Raspberry Pi Foundation, Cambridge UK) recorded the movement of the optical fiducials during motion and performed an off-line analysis to determine relative angular displacement (Fig. 5). We used filter masks to reduce

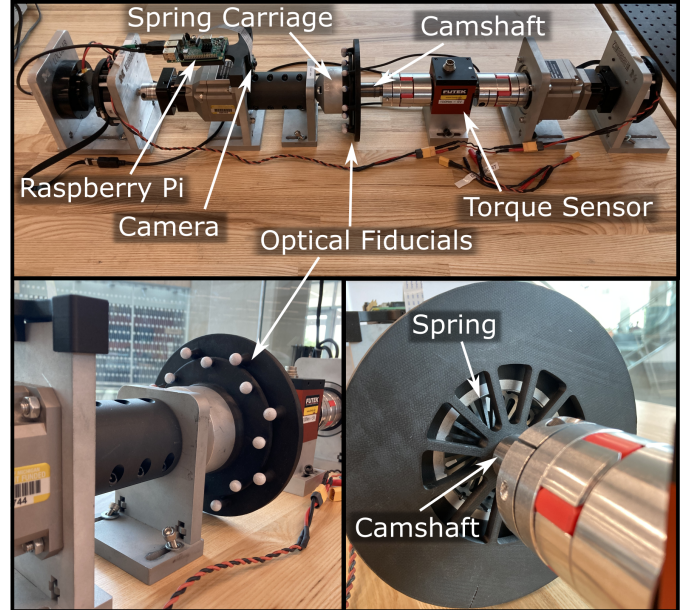


Fig. 4. Testbed used to evaluate spring performance. By tracking optical fiducials with a camera, we were able to measure true deflection of the springs.

the image to the areas of interest (the two arcs containing fiducials). Subsequently, we used OpenCV [REF] to track the fiducials in the plane of the image (Fig. 5c), and determined the displacement using best-fit ellipses obtained from a calibration procedure. The fit for the measured displacement during unloaded displacement versus the motor encoder measurement from the actuator demonstrated high accuracy ( $y = 0.9998x - 0.0709$  deg).

The testing that we performed thoroughly spanned the expected operating ranges of the springs. With each spring, we increased the deflection in one direction to a specified limit, then subsequently decreased the deflection to zero and repeated the process in the opposite direction. We began with two degrees of deflection in both directions and increased the allowable deflection in 1-2 degree steps until we reached deflections well past the designed limit. Each ramp lasted five seconds, so smaller angles of deflection also had a slower associated angular velocity. By comparing deflection and torque measurements, we quantified the torque-angle relationship of each spring and the maximum ranges of safe operation.

### B. Results

The measured performance of the springs closely matched the desired specifications. First, each spring achieves its de-

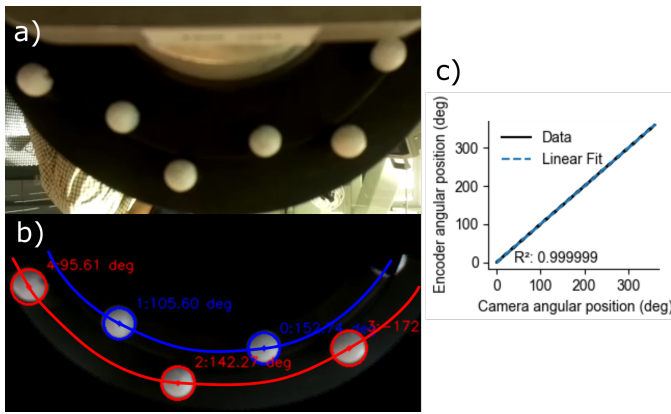


Fig. 5. Testbed used to evaluate spring performance. By tracking optical fiducials with a camera, we were able to measure true deflection of the springs.

signed deflection limits without signs of failure (Fig. 6). In addition, the measured spring rates closely align with the target spring rate (Table I), falling within 3-7% of the intended value for all three springs (Table II). We also quantified energy loss due to hysteresis during the loading and unloading process. At designed deflection (as depicted) the percent energy loss is approximately 10 percent (S1: 9.72%, S2: 12.0%, and S3: 10.9%). However, at smaller deflections of nine degrees, those percentages are dramatically lower (S1: 0.41%, S2: 1.08%, and S3: 1.50%).

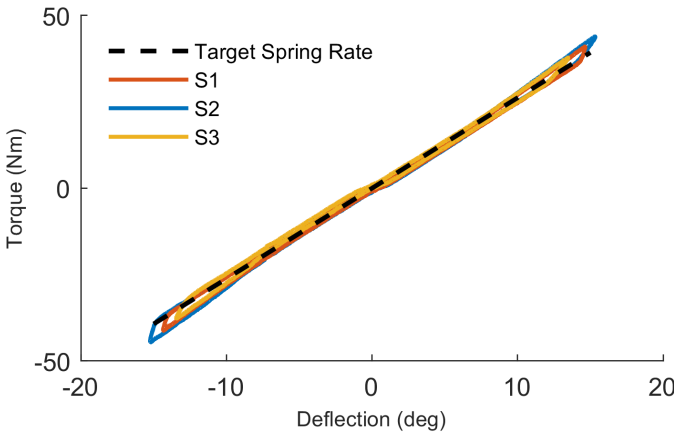


Fig. 6. Measured spring rates of S1, S2 and S3 over each spring's respective operable range. For reference, the target spring rate of 150 Nm/rad is also displayed.

TABLE II

SPRING RATES OF THE THREE SPRING DESIGNS DURING BOTH LOADING AND UNLOADING IN BOTH POSITIVE AND NEGATIVE TORQUE REGIMES. AVERAGE SPRING RATE AND PERCENT ERROR ARE ALSO REPORTED. THE DESIRED SPRING RATE WAS 150 NM/RAD FOR ALL THREE DESIGNS.

Spring Design	Spring Rate (Nm/rad)					
	Loading		Unloading		Avg.	Error (%)
	Pos.	Neg.	Pos.	Neg.		
S1	159.6	161.8	150.3	152.0	155.9	3.95
S2	165.4	165.1	155.3	151.5	159.3	6.22
S3	156.8	162.2	148.9	151.7	154.9	3.27

Though not empirically validated, we also designed our springs to last roughly 100,000 alternating cycles under full

load. Using S-N curve estimation as outlined in [31], we determined the design stress (912 MPa) that achieves 100,000 cycles with our material (SS 420). This stress limit was used as an input to the design tool when creating all four springs.

## V. DISCUSSION

### A. Contributions

Elastic elements are a critical aspect of many robotic systems, especially those that operate in close proximity with humans. In this paper, we presented the design and validation of a compact monolith spring geometry. The motivation of our exploration was to design a sufficiently compact and lightweight spring to justify integration in robotic prostheses [26]. Our design framework radically deviates from conventional designs, comprising a circular array of tapered cantilever flexures in contact with a gear-like camshaft (Fig. 7).

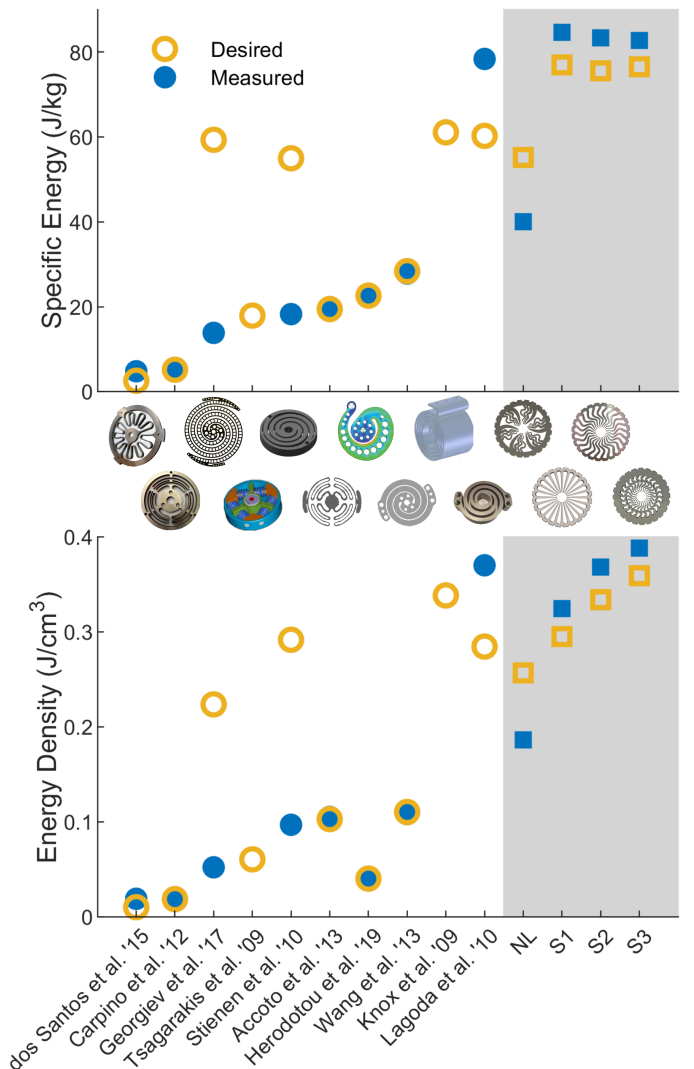


Fig. 7. Performance of cantilever-beam rotary springs (gray region) by energy storage per unit mass and per unit volume in the context of the current literature. It should be noted that the mass and volume of the S3 spring was estimated for an outer rim thickness comparable to that of S1 and S2 rather than using the unnecessarily large rim than was dictated by our testing apparatus.

Furthermore, the hardware validation that we performed demonstrates that our modeling and design is capable of producing springs that accurately achieve the desired performance. As stated in the description of the spring design, there are several assumptions that we made in the modeling phase of this project. The fact that we predicted stiffness characteristics within 3-7% implies that our design approximations were appropriate (Tab. II). This compatibility between model and physical system—coupled with the open-source spring design tool that we created—means that designers can convert a set of spring specifications into a design for an efficient spring with customized properties in a matter of minutes.

### B. Limitations

While the current state of this design does yield impressive results, there are several areas for further improvement, which could be the subject of future research endeavors. First and foremost, the hysteresis observed in the springs is significant. We predict that it is primarily due to the sliding contact between the flexures and the teeth of the camshaft, which would indicate that hysteresis may be an unavoidable drawback of this approach; however, this study did not include any attempts to confirm the source of hysteresis or lessen its effects. Possible mitigation strategies could include something as simple as lubrication on the contact faces.

To simplify fabrication and failure analysis, the current state of our design applies only to isotropic metals. We are aware of materials with higher energy storage per mass—including fiberglass and carbon fiber—and future work could focus on optimizing that design.

In addition, the spring design tool—while usable and useful—is currently limited in scope. First, it does not include the design of the camshaft. In fact, the design of the camshaft is under-formalized—the profile being chosen to maintain the proper loading condition throughout the range of motion, but selected by visual inspection using CAD software (Solidworks). Lastly, the tool optimizes for spring designs that are least likely to intersect, but this behavior is not guaranteed by the constraints. With improvements in these areas, the tool could increase in utility.

### C. Broader Applicability

This spring design is robust and highly customizable, so possible applications are vast. The most significant area of impact would likely be in mobile robots that utilize SEAs, including humanoid robots, legged robots, serial-link manipulators, prosthetic limbs, exoskeletons, etc. Prostheses and exoskeletons specifically must be tunable to the needs and requirements of the user, so quick and simple replacement of differing springs could be particularly beneficial.

Alternatively, there are many modifications or further developments that could be pursued in order to make this design even more broadly applicable. For example, the bending beam paradigm could be transformed to yield prismatic springs, which could be useful as high-efficiency alternative to springs in series with linear actuators, or in mechanisms such as suspension systems. Another possibility is to implement series

interconnections of the spring, enabling larger deflection limits of the springs [18]. Lastly, the underconstrained interface between the camshaft and the spring could be exploited to create a sliding clutch or variable spring-rate mechanism.

## VI. CONCLUSION

In this paper, we presented a novel spring design characterized by a ring of radially-extending tapered cantilever beams in contact with a gear-like camshaft. This new paradigm yields the most energy-efficient springs to date. In addition, we introduced a design tool that will facilitate rapid adoption and customization of this technology. We also tested four representative springs on a custom testbed to demonstrate the high fidelity of our design framework. This work increases the potential for incorporating springs into lightweight and compact mechanisms.

## ACKNOWLEDGMENT

## REFERENCES

- [1] G. A. Pratt and M. M. Williamson, "Series elastic actuators," in *Intelligent Robots and Systems 95.'Human Robot Interaction and Cooperative Robots', Proceedings. 1995 IEEE/RSJ International Conference on*, vol. 1. IEEE, 1995, pp. 399–406.
- [2] J. Pratt, B. Krupp, and C. Morse, "Series elastic actuators for high fidelity force control," *Industrial Robot*, vol. 29, no. 3, pp. 234–241, 2002.
- [3] C. Fitzgerald, "Developing baxter," in *Technologies for Practical Robot Applications (TePRA), 2013 IEEE Conference on*. IEEE, 2013, pp. 1–6.
- [4] K. Kong, J. Bae, and M. Tomizuka, "Control of rotary series elastic actuator for ideal force-mode actuation in human–robot interaction applications," *IEEE/ASME Transactions on Mechatronics*, vol. 14, no. 1, pp. 105–118, Feb 2009.
- [5] M. M. Williamson, "Robot arm control exploiting natural dynamics," Ph.D. dissertation, Massachusetts Institute of Technology, 1999.
- [6] G. A. Pratt, "Low impedance walking robots," *Integrative and Comparative Biology*, vol. 42, no. 1, pp. 174–181, 2002.
- [7] M. K. Shepherd and E. J. Rouse, "The vspa foot: A quasi-passive ankle-foot prosthesis with continuously variable stiffness," *TRANSACTIONS ON NEURAL SYSTEMS AND REHABILITATION ENGINEERING*, vol. 25, no. 12, pp. 2375–2386, 2017.
- [8] C. Hubicki, J. Grimes, M. Jones, D. Renjewski, A. Spröwitz, A. Abate, and J. Hurst, "Atrias: Design and validation of a tether-free 3d-capable spring-mass bipedal robot," *The International Journal of Robotics Research*, vol. 35, no. 12, p. 1497–1521, 2016.
- [9] F. Negrello, M. G. Catalano, M. Garabini, M. Poggiani, D. G. Caldwell, N. G. Tsagarakis, and A. Bicchi, "Design and characterization of a novel high-compliance spring for robots with soft joints," in *2017 IEEE international conference on advanced intelligent mechatronics (AIM)*. IEEE, 2017, pp. 271–278.
- [10] S. Yoon, S. Kang, S. Kim, Y. Kim, M. Kim, and C. Kim, "Safe arm with mr-based passive compliant joints and visco-elastic covering for service robot applications," in *2003 IEEE/RSJ international conference on intelligent robots and systems*. IEEE, 2003, pp. 2191–2196.
- [11] N. G. Tsagarakis, M. Laffranchi, B. Vanderborght, and D. G. Caldwell, "A compact soft actuator unit for small scale human friendly robots," in *2009 IEEE international conference on robotics and automation*. IEEE, 2009, pp. 4356–4362.
- [12] B. T. Knox and J. P. Schmideler, "A Unidirectional Series-Elastic Actuator Design Using a Spiral Torsion Spring," *Journal of Mechanical Design*, vol. 131, no. 12, 11 2009, 125001. [Online]. Available: <https://doi.org/10.1115/1.4000252>
- [13] A. H. Stienen, E. E. Hekman, H. ter Braak, A. M. Aalsma, F. C. van der Helm, and H. van der Kooij, "Design of a rotational hydroelastic actuator for a powered exoskeleton for upper limb rehabilitation," *Transactions on Biomedical Engineering*, vol. 57, no. 3, pp. 728–735, 2010.
- [14] C. Lagoda, A. C. Schouten, A. H. Stienen, E. E. Hekman, and H. van der Kooij, "Design of an electric series elastic actuated joint for robotic gait rehabilitation training," in *2010 3rd IEEE RAS & EMBS international conference on biomedical robotics and biomechatronics*. IEEE, 2010, pp. 21–26.

- [15] S. Wang, C. Meijneke, and H. van der Kooij, "Modeling, design, and optimization of mindwalker series elastic joint," in *2013 IEEE 13th International Conference on Rehabilitation Robotics (ICORR)*. IEEE, 2013, pp. 1–8.
- [16] N. Georgiev and J. Burdick, "Design and analysis of planar rotary springs," in *2017 IEEE/RSJ International Conference on Intelligent Robots and Systems (IROS)*. IEEE, 2017, pp. 4777–4784.
- [17] S. Yoo, J. Lee, J. Choi, G. Chung, and W. K. Chung, "Development of rotary hydro-elastic actuator with robust internal-loop-compensator-based torque control and cross-parallel connection spring," *Mechatronics*, vol. 43, pp. 112–123, 2017.
- [18] G. Carpino, D. Accoto, F. Sergi, N. Luigi Tagliamonte, and E. Guglielmelli, "A Novel Compact Torsional Spring for Series Elastic Actuators for Assistive Wearable Robots," *Journal of Mechanical Design*, vol. 134, no. 12, 10 2012, 121002. [Online]. Available: <https://doi.org/10.1115/1.4007695>
- [19] N. Paine, J. S. Mehling, J. Holley, N. A. Radford, G. Johnson, C.-L. Fok, and L. Sentis, "Actuator control for the NASA-JSC Valkyrie humanoid robot: A decoupled dynamics approach for torque control of series elastic robots," *Journal of Field Robotics*, vol. 32, no. 3, pp. 378–396, 2015.
- [20] D. Accoto, G. Carpino, F. Sergi, N. L. Tagliamonte, L. Zollo, and E. Guglielmelli, "Design and characterization of a novel high-power series elastic actuator for a lower limb robotic orthosis," *International Journal of Advanced Robotic Systems*, vol. 10, no. 10, p. 359, 2013. [Online]. Available: <https://doi.org/10.5772/56927>
- [21] W. M. dos Santos, G. A. Caurin, and A. A. Siqueira, "Design and control of an active knee orthosis driven by a rotary series elastic actuator," *Control Engineering Practice*, vol. 58, pp. 307–318, 2017.
- [22] T. Kim, K. Shi, and K. Kong, "A compact transmitted-force-sensing series elastic actuator with optimized planar torsional spring for exoskeletons taeyeon," in *2021 IEEE/ASME International Conference on Advanced Intelligent Mechatronics (AIM)*. IEEE/ASME, 2021, pp. 572–577.
- [23] G. G. Fiorezi, J. dos Santos de Moraes, P. H. Fabriz Ulhoa, and R. M. de Andrade, "Biomimetic design of a planar torsional spring to an active knee prosthesis actuator using fem analysis," in *Proc. First International Electronic Conference on Actuator Technology*. MDPI, 2020, pp. 1–11.
- [24] J. P. Cummings, D. Ruiken, E. L. Wilkinson, M. W. Lanigan, R. A. Grupen, and F. C. S. IV, "A compact, modular series elastic actuator," *Journal of Mechanisms and Robotics*, vol. 8, pp. 1–11, 2016.
- [25] P. Herodotou and S. Wang, "Design, modelling, and experimental evaluation of a compact elastic actuator for a gait assisting exoskeleton," in *2019 IEEE 16th International Conference on Rehabilitation Robotics (ICORR)*. IEEE, 2019, pp. 331–336.
- [26] A. F. Azocar, L. M. Mooney, J.-F. Duval, A. M. Simon, L. J. Hargrove, and E. J. Rouse, "Design and clinical implementation of an open-source bionic leg," *Nature Biomedical Engineering*, vol. 4, no. 10, pp. 941–953, 2020.
- [27] L. Mooney, K. A. Pasch, and T. D. Doan, "Planar torsion spring for knee prostheses and exoskeletons," Aug. 24 2017, uS Patent App. 15/402,186.
- [28] M. K. Shepherd and E. J. Rouse, "Design and validation of a torque-controllable knee exoskeleton for sit-to-stand assistance," *TRANSACTIONS ON MECHATRONICS*, vol. 22, no. 4, pp. 1695–1704, 2017.
- [29] B. J. Goodno and J. M. Gere, *Mechanics of Materials, Ninth Edition*. Cengage Learning, 2013.
- [30] E. A. Bolívar-Nieto, G. C. Thomas, E. Rouse, and R. D. Gregg, "Convex optimization for spring design in series elastic actuators: From theory to practice," in *2021 IEEE/RSJ International Conference on Intelligent Robots and Systems (IROS)*. IEEE, 2021, pp. 9327–9332.
- [31] J. A. Collins, H. Busby, and G. Staab, *Mechanical Design of Machine Elements and Machines, Second Edition*. Wiley, 2010.